NASA/TM—2009-215625

Flowability of JSC-1a

Enrique Rame
National Center for Space Exploration Research, Cleveland, Ohio

Allen Wilkinson
Glenn Research Center, Cleveland, Ohio

Alan Elliot
University of Kansas, Lawrence, Kansas

Carolyn Young
Case Western Reserve University, Cleveland, Ohio

May 2009

NASA STI Program . . . in Profile

Since its founding, NASA has been dedicated to the advancement of aeronautics and space science. The NASA Scientific and Technical Information (STI) program plays a key part in helping NASA maintain this important role.

The NASA STI Program operates under the auspices of the Agency Chief Information Officer. It collects, organizes, provides for archiving, and disseminates NASA's STI. The NASA STI program provides access to the NASA Aeronautics and Space Database and its public interface, the NASA Technical Reports Server, thus providing one of the largest collections of aeronautical and space science STI in the world. Results are published in both non-NASA channels and by NASA in the NASA STI Report Series, which includes the following report types:

- TECHNICAL PUBLICATION. Reports of completed research or a major significant phase of research that present the results of NASA programs and include extensive data or theoretical analysis. Includes compilations of significant scientific and technical data and information deemed to be of continuing reference value. NASA counterpart of peer-reviewed formal professional papers but has less stringent limitations on manuscript length and extent of graphic presentations.

- TECHNICAL MEMORANDUM. Scientific and technical findings that are preliminary or of specialized interest, e.g., quick release reports, working papers, and bibliographies that contain minimal annotation. Does not contain extensive analysis.

- CONTRACTOR REPORT. Scientific and technical findings by NASA-sponsored contractors and grantees.

- CONFERENCE PUBLICATION. Collected papers from scientific and technical conferences, symposia, seminars, or other meetings sponsored or cosponsored by NASA.

- SPECIAL PUBLICATION. Scientific, technical, or historical information from NASA programs, projects, and missions, often concerned with subjects having substantial public interest.

- TECHNICAL TRANSLATION. English-language translations of foreign scientific and technical material pertinent to NASA's mission.

Specialized services also include creating custom thesauri, building customized databases, organizing and publishing research results.

For more information about the NASA STI program, see the following:

- Access the NASA STI program home page at *http://www.sti.nasa.gov*

- E-mail your question via the Internet to *help@sti.nasa.gov*

- Fax your question to the NASA STI Help Desk at 301–621–0134

- Telephone the NASA STI Help Desk at 301–621–0390

- Write to:
  NASA Center for AeroSpace Information (CASI)
  7115 Standard Drive
  Hanover, MD 21076–1320

NASA/TM—2009-215625

Flowability of JSC-1a

Enrique Rame
National Center for Space Exploration Research, Cleveland, Ohio

Allen Wilkinson
Glenn Research Center, Cleveland, Ohio

Alan Elliot
University of Kansas, Lawrence, Kansas

Carolyn Young
Case Western Reserve University, Cleveland, Ohio

National Aeronautics and
Space Administration

Glenn Research Center
Cleveland, Ohio 44135

May 2009

Level of Review: This material has been technically reviewed by technical management.

Available from

NASA Center for Aerospace Information
7115 Standard Drive
Hanover, MD 21076–1320

National Technical Information Service
5285 Port Royal Road
Springfield, VA 22161

Available electronically at http://gltrs.grc.nasa.gov

Flowability of JSC-1a

Enrique Ramé
National Center for Space Exploration Research
Cleveland, Ohio 44135

Allen Wilkinson
National Aeronautics and Space Administration
Glenn Research Center
Cleveland, Ohio 44135

Alan Elliot
University of Kansas
Lawrence, Kansas 66045

Carolyn Young
Case Western Reserve University
Cleveland, Ohio 44106

Abstract

We have done a complete flowability characterization of the lunar soil simulant, JSC-1a, following closely the ASTM-6773 standard for the Schulze ring shear test. The measurements, which involve pre-shearing the material before each yield point, show JSC-1a to be cohesionless, with an angle of internal friction near 40°. We also measured yield loci after consolidating the material in a vibration table which show it to have significant cohesion ($\approx$ 1 kPa) and an angle of internal friction of about 60°. Hopper designs based on each type of flowability test differ significantly. These differences highlight the need to discern the condition of the lunar soil in the specific process where flowability is an issue. We close with a list –not necessarily comprehensive– of engineering rules of thumb that apply to powder flow in hoppers.

1 Introduction

Lunar exploration's goal of establishing a long-term human presence will require considerable movement of lunar regolith for applications ranging from road and habitat construction to mining the regolith for chemical processing. To complete these activities successfully, systems highly dependent on how the bulk soil "flows" (or fails, if the operation's success cannot allow the soil to flow) must be properly designed. This is a non-trivial challenge, not only because "flow" of lunar soil has not been closely examined in the past, but also –and more importantly– because constitutive models of granular or "bulk solids" are not available with the same fidelity as, say, those of liquids or simple conventional solids.

Depending on the goal of a particular operation, flow of a bulk granular solid is either desired or is to be avoided. For example, a foundation must be large enough that the stresses exerted on the soil are always smaller than the soil's failure strength. By contrast, mined soil stored in a bin must be guaranteed to flow out of the hopper when the discharge valve opens. Here, the stresses at the hopper outlet must be higher than the soil's strength.

No matter what flow regime or system (or "operation", in the chemical engineering jargon), flow of a bulk granular solid is likely to play a role at some point during the process. Excavator arms must be designed mechanically so they can deliver the force necessary to penetrate, then scoop out and dump the soil, all of which are highly dependent on soil flow properties. Starting up a gas-fluidized bed requires that the gas drag on the particles exceed the bulk granular material strength achieved through consolidation by self-weight, vibrations or other means (gas flow through the bed after startup is of course an issue, but is not the focus of this study). If the bed is fluidized by oscillations instead of gas, the inertial force caused by the oscillatory acceleration must overcome the soil strength homogeneously. During flow, assemblies of grains may segregate or mix, depending on grain properties, flow regime and geometry of flow device. Thus, it must be clear that "flow" of bulk granular material involves the study of how forces exerted on the material (by bounding walls, tools, viscous drag from the gas or the solid's own weight) affect the onset, evolution and arrest of flow, and, conversely, what are the forces a flowing or static bulk granular material exerts on the solids (tools or bounding walls) in contact with it. The proper design of storage bins, of mechanical diggers, movers and conveyors, of tires and wheels, all depend on the forces cited above. Hence, the engineering importance of granular flow phenomena cannot be neglected.

In the flow examples cited above, each particle interacts with many particles through simultaneous contacts, the extreme case being "quasi-static" flows where the particles evolve through a sequence of static equilibrium states as they flow. These flows are characterized by high solids volume fractions. There are other flow regimes where each particle interacts with only one other particle at a time during flow; these are known as "collisional flows". Collisional flows are characterized by lower solids fraction than quasi-static flows and prevail in highly agitated situations such as fluidized beds, chutes and catalytic crackers. In this work, we apply Jenike's classical ideas of flowability [1] to quasi-static flows, and adhere closely to ASTM standard methods to assess the flowability of JSC-1a, a lunar soil simulant, and, eventually,

compare it to that of actual lunar regolith.

Bulk granular materials (of which soils, regolith and simulants are examples) are composed of microscopic to macroscopic grains (or particles) with a certain size distribution, composition and morphology. Their response to stress is extremely sensitive to small changes in their properties, e.g., water content, density, size distribution, shape, surface roughness, friability. Not surprisingly, handling bulk granular materials poses significant challenges as evidenced by the disproportionately high failure rate of terrestrial bulk handling equipment as compared to hardware for handling fluids. The crucial problem is that the tools that predict their mechanical behavior are not as well grounded as, for example, those for conventional, non-granular solids and fluids. It is estimated that bulk granular solids handling processes operate at about 63 % capacity; a significantly lower efficiency than fluid-dependent processes which operate at about 84 % capacity [2]. With this background, Wilkinson *et al.* summarize knowledge gaps and likely technological difficulties specifically focused on lunar and Martian processes [3].

Depending on the stress level exerted on them, bulk granular solids can exhibit behaviors that resemble closely a solid or a fluid. The solid-to-fluid transition is controlled by the strength of the bulk material. Loosely speaking, when the applied stress exceeds the strength, the material fails and begins to "flow" much in the same way as a liquid. This failure is not too different from abrupt failure of conventional solids (metals, wood) but it is peculiar in that the strength of the granular material is itself a function of the stress imposed on it, even when the path to failure is "quasi static" deformation. In spite of the difficulties posed by their characterization, bulk granular solids are commonly and successfully used in terrestrial applications ranging from oil refineries to pharmaceutical processes, agriculture and civil engineering work; and engineering design rules have been developed to guide designs involving granular bulk solids [1, 4].

A lot of work has been done to characterize the mechanical properties of lunar regolith returned to Earth with Apollo missions [5–12]. Although this work is rather comprehensive, the systematic, standard tests needed to complete a hopper design are not available. Nelson [13] found that the porosity of soils depends non-monotonically on the atmospheric pressure; at low vacuum levels, the porosity decreased, while at high and ultra-high vacuum it increased. Clearly, dominant interparticle forces change drastically with vacuum level. Nicholson [14], and Pariseau & Nicholson [15] devised a torsional (or rotational) shear cell, conceptually similar to the Schulze ring shear tester prescribed in the ASTM 6773 standard; but their strength measurements do not subject the sample to "pre-shear" as this standard calls for to address flow. More recently, the lunar simulant MLS-1 has been characterized mechanically [16]; and JSC-1a has been characterized rather comprehensively for mechanical and physical properties –but not for flowability [17, 18].

For engineering applications on the Moon, one should be aware that flowability measurements on Earth may not represent well the prevailing gravitational consequences on the Moon. If the powder strength depends only on normal load, then it is easy to adjust (i.e., reduce) this force on Earth to mimic the corresponding load on the Moon. However, should the material strength depend also on the normal load gradient (given approximately by $\rho_b g$, where ρ_b is bulk density), a terrestrial

experiment cannot reproduce lunar conditions and the strength determination may be questionable.

The rate of flow of a bulk granular material through a circular orifice has been modeled traditionally by the Beverloo law [19]. In their recent paper, Mankoc *et al.* [20] review this model critically and propose an improvement based on careful data analysis of experiments and Discrete Element Modeling (DEM) simulations. Along these lines, a trend is rapidly developing in industry to establish more advanced methods for predictive models and simulation [21].

In this paper we examine the classical flowability (see, e.g., [1]) of the lunar simulant JSC-1a as it applies to its ability to flow out of a hopper where the material would be stored; thus, modeling flow rate behavior is beyond the scope of this study. Classical flowability measures the relative ease with which a bulk material "flows", specifically slow, high-solid fraction flows –which are markedly different from the highly agitated, much less dense flows such as chute flows, gas-driven flows and collisional flows.

Given a material stored in a silo or bin, say, the onset of flow depends on intrinsic, history-dependent powder strength properties, powder-hopper wall friction, and hopper geometry, i.e, orifice size and cone angle. Knowing the powder material and hopper wall material, the design consists of determining the hopper's cone angle and orifice size that guarantees powder flow when the discharge valve opens. In this work we perform a complete characterization of JSC-1a from the classical flowability point of view, from powder strength to powder-wall friction. With these data, we then design a hopper following the method of Jenike [1]. This type of characterization of JSC-1a can offer a basis of comparison with the flowability of actual lunar soil and, at the same time, assist in the future development of suitable simulant requirements related to flow.

1.1 Brief introduction to powder flowability and its impact on hopper design

In order for the material to be set in flow, the applied stress must exceed the powder strength. It follows that there is a certain shear stress that must be exceeded before the powder will flow. This critical shear stress is called "failure shear", τ_f, and, for all practical systems, increases monotonically with σ.

The central measurement of powder strength is known as the "yield locus" and is shown schematically in fig. 1. In each yield locus, the powder is first subjected to a normal "pre-consolidation pressure", σ_c, which is higher than each of the normal loads used in the individual yield points and then pre-sheared to steady state at the pre-consolidation pressure. The test proceeds by applying a sequence of decreasing normal loads σ_i, with $\sigma_c > \sigma_1 > \sigma_2...$, and failing the material at each σ_i, with a steady-state pre-shear preformed under $\sigma = \sigma_c$ between σ_i and σ_{i+1}.

The yield locus is interpreted using the Mohr-Coulomb theory [22]:

$$\tau_f = c + \tan\phi\ \sigma, \tag{1}$$

where c is cohesion and ϕ is angle of internal friction. These are empirical quantities (i.e., not material properties) that are not independent of each other or the history of

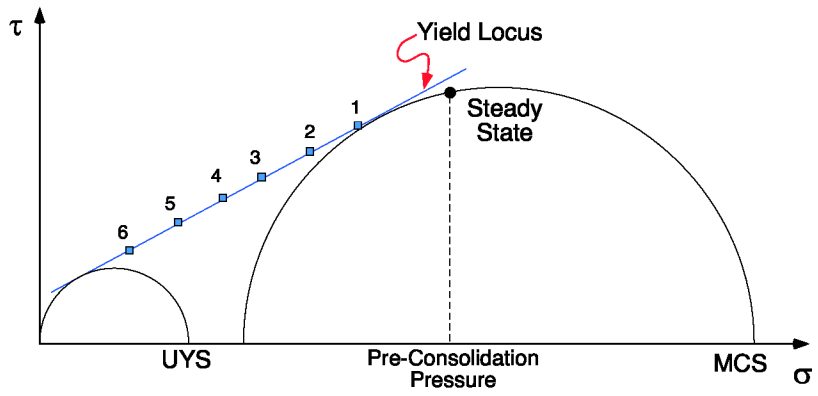

Figure 1: Schematic of yield shear versus normal load for a given consolidation pressure showing the steady-state pre-shear and the yield points (squares 1 to 6). The Mohr circles determine the major consolidation stress (MCS) and unconfined yield strength (UYS). Admissible yield locus points must be between the two circles' tangency points to the yield locus line.

the sample. Each point on the yield locus corresponds to a state of stress at failure in the powder. This may be seen by assuming a 2D stress state and using a Mohr circle [23] that is tangent to the yield locus line. Such a Mohr circle is a "failure circle". The tangency point represents the shear and normal stresses at the failure plane of the yield locus, $[\tau_f, \sigma]$. Any other pair of $[\tau, \sigma]$ on the circle represents the shear and normal stresses on another plane in the solid consistent with the same stress state in the solid. Thus, any pair of stresses on that circle will cause failure in a manner identical to $[\tau_f, \sigma]$.

The "cohesion" is the shear that must be applied to make the powder flow even in the absence of normal load; and $\tan\phi$ is the slope of the straight line fit to the experimental yield locus points. When $c = 0$, $\tan\phi = \tau_f/\sigma$ is a "friction coefficient"; when $c \neq 0$, the friction coefficient, defined as τ_f/σ, is $\tan\phi + c/\sigma$ i.e., it depends on the normal load. Interestingly, measuring a value for $c \neq 0$ does not necessarily imply that a powder's particles have "cohesive (or tensile) strength" between them arising from, e.g., cementation, electrostatic or other forces. In fact, a powder with no interparticle tensile strength may show effective cohesion, $c \neq 0$, in a yield locus test due to morphology and/or broad size distribution effects.

For each yield locus, the "unconfined yield strength" (UYS) and the "major consolidation stress" (MCS) may be computed or found graphically [1] (see Appendix for exact formulae). The UYS is the major principal stress when the powder is under failure conditions and the principal minor stress is zero (that is, the sample is unconfined). The MCS is the major principal stress in the material when the consolidation pressure is applied and the material is at the onset of failure (or flow). Fig. 1 shows a graphical construction to find the UYS and MCS. A plot of UYS vs. MCS for a set of pre-consolidation loads is called "flow function" and constitutes a first measure of flowability. The slope of such a plot is the "flow index"; the higher the flow index, the less flowable the powder.

Cohesion of JSC-1 has been measured by Boles *et al.* [24] using the triaxial test

method (ASTM D2850, D4767). In this test, the major principal stress at failure is measured for each minor confining stress, and a 'failure' Mohr circle may be constructed from the two principal stress values. In the cited work, and using three confining stresses, the Mohr circle straight failure envelope intersects the vertical axis with a cohesion of about 1 kPa. This value is not justified because none of the accepted criteria for real or apparent cohesion are met. In particular, the authors discount apparent cohesion from geometrical (or shape-driven) friction because their SEM images of particle surfaces do not appear sufficiently rough to generate interlocking. While the particles may well lack significant roughness, shape-driven apparent cohesion may still arise if interparticle contacts are present along a plane not parallel to the shear force. The triaxial test's inability to access low enough normal forces is noted as a probable cause of inaccuracy in the measured cohesion. This forces the practitioner to extrapolate the failure envelope back to zero normal load over a large range of normal loads. Since it is well known that actual yield loci are curved, especially near $\sigma = 0$, the extrapolation to zero σ needed in the triaxial test method is of questionable validity [25, 26]. Further, Boles' good mechanical characterization did not have the series of systematic measurements needed to evaluate flowability.

Proper design of hoppers is crucial because lunar regolith will likely be stored in bins fitted with a discharge hopper until it is needed in an industrial process. At some point, a controlled amount and flow rate of regolith must be discharged from the bin onto an appropriate transportation medium (e.g., conveyor, chute, truck). Ideally, a hopper must be designed to ensure "mass flow" of the powder, a condition in which *all* of the powder mass is in motion. By contrast, in "funnel flow" the powder in the center of the hopper flows, while material adjacent to the walls remains motionless or flows more slowly. Mass flow is more desirable for several reasons, among them: a) funnel flow onset is more difficult to predict than mass flow onset; b) funnel flow leads to more segregation than mass flow, which creates control issues in the equipment (e.g., a reactor) using the powder. The transition between flowing and non-flowing powder –and thus, hopper design– depends critically on the powder strength and powder-wall friction. The hopper design method developed by Jenike [1] requires a certain series of measurements of powder strength and powder-wall friction. Though lunar simulant has been characterized before mechanically quite thoroughly, the series of measurements needed for hopper design has never been performed.

In this paper, we fail the JSC-1a simulant in a shear rotational cell following closely the ASTM 6773 standard developed for the Schulze ring shear cell.[1] We carry out all the series of tests required in the hopper design method of Jenike [1]. Compared to the triaxial test, the ring shear test has the following main advantages:

1) It allows application of smaller normal loads ($\approx$ 0.5 kPa) and, thus, enhances the quality of the low-σ extrapolation that determines cohesion. In a typical triaxial test, the smallest normal stress on the failure plane is about 150 kPa [17].

2) It measures directly the shear failure at each normal load, thus eliminating the need for drawing Mohr circles to determine the failure envelope. Accessing the low-normal load region of the yield locus is crucial for flowability design of hoppers, as the range of critical stress at the onset of flow is also low.

[1]Since we use a different instrument from the Schulze Ring Shear Tester, our experiments strive to adhere to but do not strictly follow the ASTM 6773 standard

2 Materials and methods

Our test bulk material is the standard (not fines, not coarse) JSC-1a lunar simulant. JSC-1a is mainly crushed basalt, with nearly 50% of SiO_2. It is mined from a volcanic ash deposit in the San Francisco volcano field near the Merriam Crater outside of Flagstaff, Arizona. Its mineral properties are summarized in the MSDS [27], produced by Orbitec Corp., the manufacturer of JSC-1a. About 500 g of JSC-1a's "Ton 2" lot was put into a glass jar by scooping it from the plastic pails where it was packaged. This procedure was carried out in a negative pressure hood for safety. The glass jar was used as the source of test powder and as the sink for used (tested) powder. Given the large number of tests we ran and the remixing between untested and tested powder, all of the powder in our possession must be considered "used". However, our extensive repetitions of tests did not suggest any measurable use effect.

2.1 Brief summary of the test method

Four types of test were performed: 1) Static yield; 2) Static yield with time consolidation; 3) Dynamic yield and 4) Wall friction. All the tests measure powder shear failure, except the wall friction which measures powder-wall shear failure. The test was performed on a commercial apparatus, ShearScan TS-12 produced by Sci-Tec Inc. (http://www.sci-tec-inc.com/). This instrument follows closely the ASTM-6773 standard. The shear failure test consists of applying a fixed angular deformation rate to the powder contained between two concentric rings while the shear stress transmitted by the powder is monitored. Once the powder is loaded in the annular sample volume, an annular lid is placed on the free surface of the powder; refer to fig. 2. The lid has vanes attached to its lower surface, sticking down about 2 mm. As the lid is lowered, these vanes sink into the powder. A motorized head simultaneously exerts a vertical force on and rotates the lid at a fixed angular velocity. The torque transmitted by the powder during this deformation is recorded. During the early stages of deformation, the torque grows linearly with the sample's angular displacement, indicating "Hookean" behavior of the bulk material. After a certain deformation, the torque growth rate decreases and the torque quickly reaches a peak. Continued deformation past the peak weakens the material, and the torque reaches a steady-state plateau below the peak level. At this point, the powder is in "failure" and "flows" in a manner similar to fluids, i.e., the material deforms with no increase in the stress needed to maintain the deformation rate. Depending on the initial relative density[2] before failure, the powder undergoes more or less significant dilation as it goes through failure.

2.2 Filling the cell and sample preconditioning

A cell measuring about 6 cm OD and 3 cm ID was filled carefully with JSC-1a contained in a glass jar adhering to the practice described in ASTM-6773. We used a

[2]For each powder, the bulk density ρ_b can take on values between a maximum and a minimum, $\rho_{b_{min}} \leq \rho_b \leq \rho_{b_{max}}$. The relative density ρ_r is defined as $\rho_r \equiv \rho_b - \rho_{b_{min}} / \rho_{b_{max}} - \rho_{b_{min}}$. Thus, $0 \leq \rho_r \leq 1$.

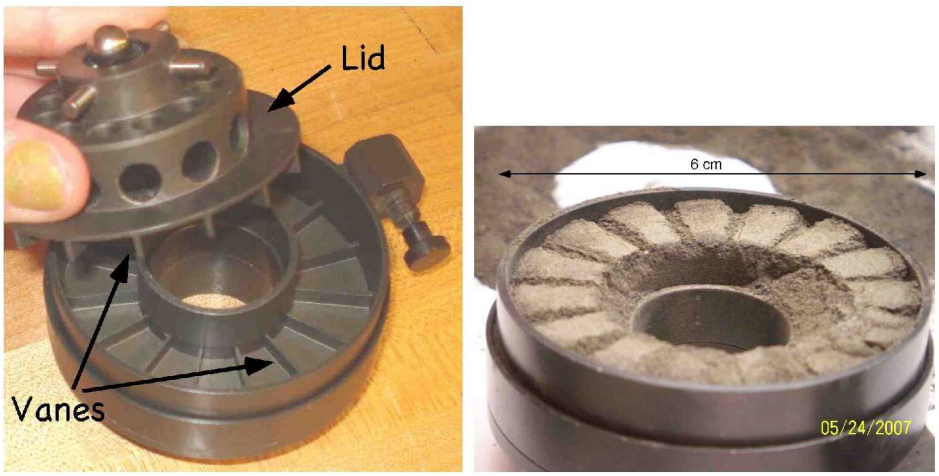

Figure 2: Photographs of the shear cell showing the annular sample volume, the lid, and the vanes attached to the lid and cell floor. A bearing ball placed at the top of the lid (left) helps transmit a vertical force applied by the instrument's vertical head. The four pegs spaced at 90 degrees around the lid top allow the instrument's vertical head to rotate the lid. The powder surface (right) shows the marks of the lid vanes after testing.

chemical spatula to scoop powder out of the jar into a funnel with a long and narrow discharge tube. The lower orifice in the funnel discharge almost touched the cell's bottom (or the powder free surface if there were powder in the cell). With powder in the funnel, the funnel was raised slightly to allow the powder to flow out, striving to ensure a uniform distribution of the powder in the cell. The process continued until the cell is overfilled. We then used a knife with a straight edge to level the material with the upper rings' edges.

After the cell is filled, the sample may be time-consolidated by a prescribed method before testing, or run immediately with pre-consolidation done while the test is running the "pre-shear steady state". In this study, we used two different time-consolidation procedures: 1) stationary consolidation in the ShearScan apparatus; and 2) consolidation on a vibration table. After a sample has been time-consolidated, it may be tested in two different ways: a) as prescribed in the ASTM-6773, the sample is put in "steady state pre-shear" at the pre-consolidation pressure before taking it to failure at the yield normal load; or b) using a non-standard method where the time-consolidated sample is taken to failure directly without pre-shear. Time-consolidation tests should reveal more closely the strength of the powder stored in a bin for some time. Samples that were not time-consolidated were subjected to the test with pre-shear pre-consolidation in the shear ring cell, as the ASTM-6773 prescribes. These represent flow conditions from freshly filled bins or hoppers.

2.2.1 Time consolidation in vibration table

Time-consolidation is performed to increase the sample's bulk density. Differences in shear failure response for different levels of pre-consolidation should hint at how

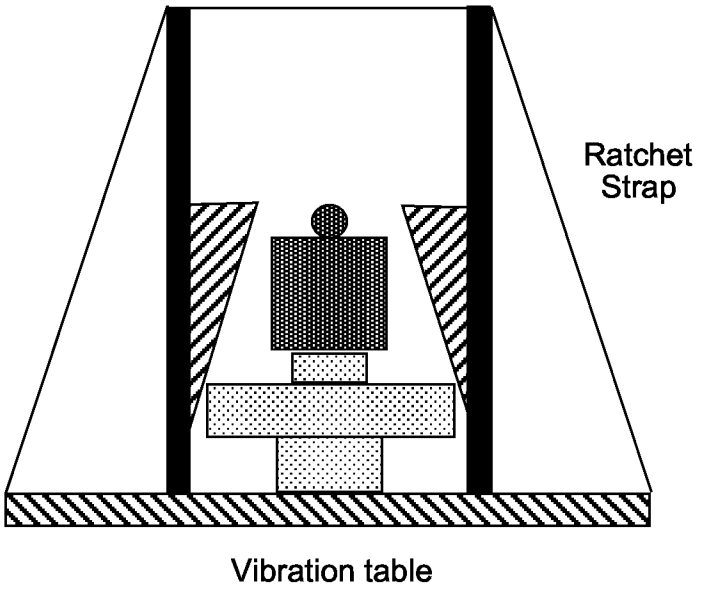

Figure 3: Schematic of the vibration table system. The shear cell is shown as lightly dotted below the weight. Two wedges are forced between the cell and the PVC pipe (solid black) to hold the cell against the pipe. The pipe is clamped to the vibration plate by means of a ratchet strap. An appropriate weight provides the consolidation stress.

significant the flow differences could be, and the difficulties vibrations could induce on the moon.

Time-consolidation was done in a FMC-Syntron's electromagnetic vibrating table model VP-51. This table vibrates vertically by flexing the plate, with maximum amplitude at the plate's periphery (manufacturer's private communication). In order to ensure an efficient vibration, the sample must not jump on the table, while the consolidation pressure remains applied. To this end, the sample cell was housed inside a PVC pipe with a 8 mm thick wall and pinned to the pipe using wood wedges placed between the pipe's inside wall and the test cell. The pipe height was sufficient that the weight could be placed in the pipe without sticking out. Then the pipe-cell assembly was strapped down to the vibrating table using a ratchet strap (see fig. 3). While the sample cell did not bounce during vibration, the weight sitting on it did. Since we cannot estimate the force the weight exerts on the sample while it bounces, we quote a nominal "consolidation pressure" as the ratio of the true weight and the powder free surface area.

2.3 Wall yield locus

This test measures the yield loci between powder and bin/hopper wall materials. It was carried out in the same cell as the conventional yield locus, except that the lid has been fitted with an annular coupon made out of the same wall material and finish as the hopper. The wall yield locus was analyzed as the conventional yield locus. The intercept of the extrapolated fit is often called "adhesion", and its angle from

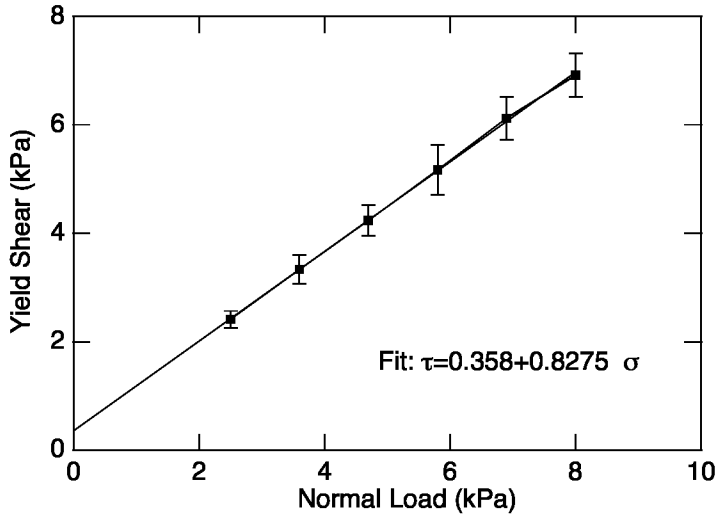

Figure 4: Static yield locus with consolidation at $\sigma_c = 10$ kPa showing averages of 10 tests at each yield point with error bars. Cohesion is ≈ 0.36 kPa and $\phi \approx 39.7°$.

the abscissa "angle of wall friction". These friction measurements can also be used to determine tool-soil forces needed in excavation work.

2.4 Data analysis

From each static powder yield locus one can obtain: cohesion, angle of internal friction, MCS, UYS. At a minimum, we performed nine repetitions (ten in most of the tests) of each data point in order to have statistical information. The data were then used to design a hopper according to the method of Jenike [1] (see §6).

3 Results

3.1 Static Yield-Locus without time consolidation

In tests without time-consolidation, the test cell filled with powder was put directly in the test apparatus. Fig. 4 shows the yield locus for pre-consolidation pressure $\sigma_c = 10$ kPa. The averages and error bars correspond to ten tests performed at each point. Fig. 5 shows a typical time trace for a single yield locus. The plot shows, as a function of time, the normal and shear stresses, and the vertical head displacement. A positive (negative) slope in the head displacement curve indicates that the head is moving down (up). From this curve one can identify sample compaction and dilation events. Using fig. 5 we now illustrate the sequence of events leading to a complete yield locus. In the first step ($t < 760$sec) the sample is brought to a steady-state pre-shear (failure) at the pre-consolidation pressure, $\sigma_c = 10$ kPa. The steady failure is identified by the steady value –within bounds– of the three variables (shear and normal stress, vertical head position). The purpose of the steady state is to ensure

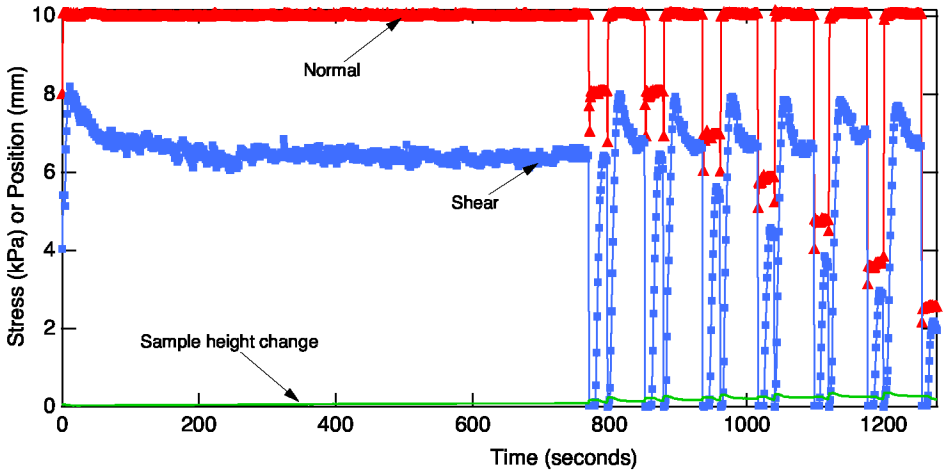

Figure 5: Time trace of a yield locus run. Consolidation $\sigma_c = 10$ kPa. ▲: Normal load. ■: Shear load. Each successive yield shear event is done at a smaller normal load, and is preceded by a steady-state preshear at the consolidation load of 10 kPa.

that all yield points are measured from a similarly prepared sample having density (or consolidation) that is uniform within the sample and similar across samples before each yield point. Once the steady "flow" is achieved, the rotation stops and the normal force retreats to zero for an instant; immediately after, the normal force σ_1, corresponding to the first yield point, is applied simultaneously with the rotation. The transmitted shear is measured; it first grows from zero (more or less linearly with the deformation), then reaches a maximum, then drops slightly to the "ultimate strength". The maximum shear stress is called the "shear failure", denoted as τ_f. After the shear failure is detected, the rotation stops and the normal force retreats for an instant. Immediately after, the pre-consolidation pressure is applied and the steady-state pre-shear preparation restarts. After the sample achieves a new "steady state" flow the normal load, σ_2, corresponding to the second yield point, is applied; the second shear failure is then found. The cycle of seady-state/yield-point continues for the rest of the yield points. The ASTM standard requires that $\sigma_1 = \sigma_2$; with progressively lower σ_i for $i > 2$. Usually, $0.2\,\sigma_c \leq \sigma_i \leq 0.8\,\sigma_c$.

3.2 Time-consolidation yield locus

In order to determine the effect of consolidation on flowability, we consolidated the sample in two ways. The first one followed the ASTM standard and is done by leaving the sample in the ShearScan apparatus for a period of time. In the second one, we consolidated using vibration. ASTM time-consolidation, (performed while the sample is in the ShearScan apparatus) does not exhibit significant differences from the yield values without time consolidation. Fig. 6 shows a yield locus for a 20-minute period of time consolidation. It falls within the highest and lowest static yield locus lines without time consolidation. We have verified that the length of time consolidation does not play a role for times less than 2.5 hours.

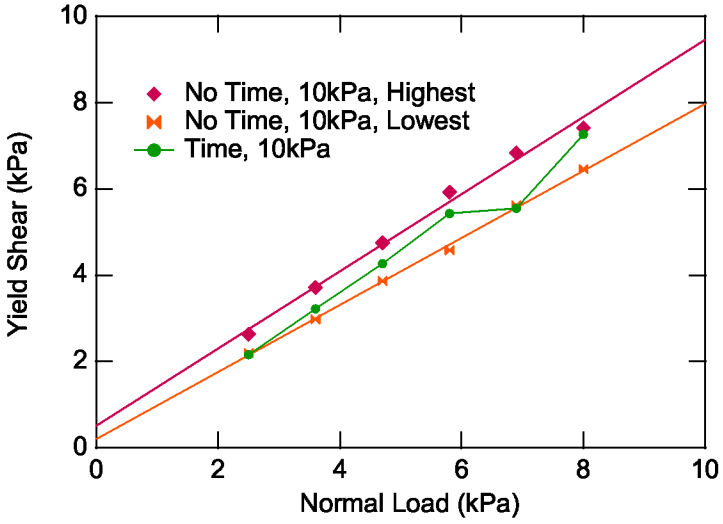

Figure 6: Static yield locus with 20-min time consolidation at $\sigma_c = 10$ kPa. The time YL is bounded by the highest and lowest static YL without time consolidation.

For vibration consolidation, the vibration time was 3 minutes and the amplitude dial in the FMC vibrating table was set at 5 (the midpoint in the dial). For all vibrations, the time was set at 3 minutes and the amplitude dial at 5. With these settings, the vibrating table yields bulk densities after consolidation between 1.8 and 2 ± 0.05 g/cm^3. (Although the bulk densities vary from test to test, we do not detect a systematic variation with consolidation stress, see table 3.) This is significantly higher than the bulk density of material poured freely into the shear cell, which ranges from 1.5 to 1.65g/cm^3. Once the sample has been consolidated in the vibration table, it was brought to the ShearScan apparatus and taken to failure at a normal pressure σ_i corresponding to the i-th yield point in the yield locus. Fig. 7 shows typical failure plots for $\sigma_c = 10$ kPa, $\sigma = 6.9$ kPa for time consolidation performed in the ShearScan and on the vibration table. In the former, the pre-consolidation pressure is applied in the ShearScan apparatus by the normal load head. In the vibration-consolidated sample, the pre-consolidation pressure is applied by a 2 kg weight placed as shown in fig. 3. The differences between the two failure plots are quantitative and qualitative. First, the shear at failure for the vibration-time-consolidated sample is considerably higher, about 5 times higher, than for the conventionally failed sample. Second, the shape of the shear stress vs. time lines are qualitatively different. The ASTM-failed sample exhibits a single regime of τ vs time, with two plateaus before reaching τ_f (the two-plateau structure does not appear in every test; a one-plateau evolution to failure is also possible). In contrast, the vibration-time-consolidated sample seems to have two regimes. The first regime looks similar to the conventional sample, with τ rising from zero and developing a first plateau. Then, instead of reaching a maximum τ and failing, the time-consolidated sample starts a second stage (beginning at ~ 30 seconds in fig. 7) where τ continues to rise at a much larger rate ($d\tau/dt$) than in the initial stage. This second stage is accompanied by a considerable dilation of the sample as

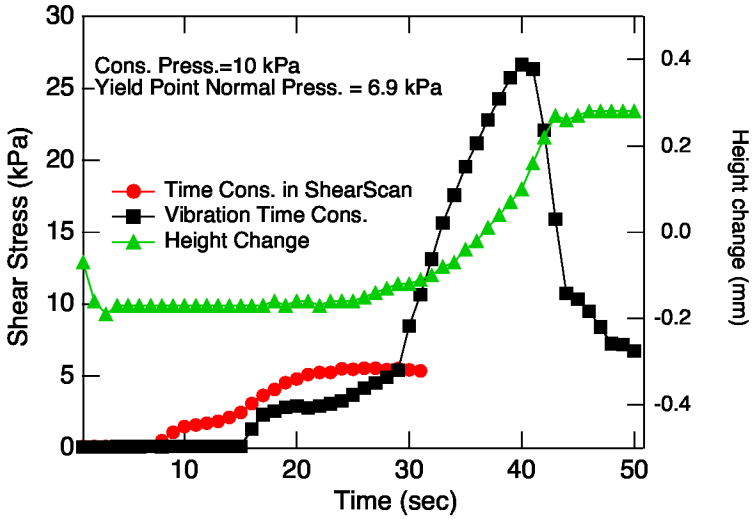

Figure 7: Shear stress at $\sigma_c = 10$ kPa, and $\sigma = 6.9$ kPa. ■: 3-minute consolidation in vibration table. ●: 20-minute consolidation in Shear Scan. ▲: height change of the vibrated sample during failure (the zero height is arbitrary).

shown in fig. 7 by the green plot of the vertical head position. It appears that the strength enhancement necessitates the sample's dilation to allow particle layers to move past each other. A few vibration-consolidated samples did not show the second stage in the strength development (probably due to defects during the vibration-consolidation stage) and did not expand dramatically during their deformation to failure, either.

In order to gather statistical data for the vibration-consolidated YL, we repeated each yield point 10 times. Fig. 8 shows a typical YL for $\sigma_c = 10$ kPa. Despite the relatively high spread (to be expected given that the sample is not preconditioned in steady-state pre-shear before failure), the plot shows convincingly a cohesion of about 1.84 kPa (compare with 0.36 kPa for conventionally failed samples at $\sigma_c = 10$ kPa). The angle of internal friction, at about 57°, is also higher than in the conventionally failed samples ($\approx 40°$). When the yield locus is performed with $\sigma_c = 20$ kPa, then $c \approx 5$ kPa and $\phi \approx 65°$. This shows how c and ϕ depend on pre-consolidation load and bulk density.

3.3 Dynamic yield locus

While in the "static yield locus" each yield point starts with a static (i.e., non-flowing) sample, the "dynamic yield locus" measures τ as a function of σ when the sample is continually flowing while σ decreases in time. The "static" and "dynamic" yield points differ much in the same way as "static" and "dynamic" friction of a block sliding on a table. The force, tangent to the table, needed to put the block in motion for a given normal load is the "static" friction force; whereas the tangent force needed to continue motion once it has started, for continually varying normal loads is the

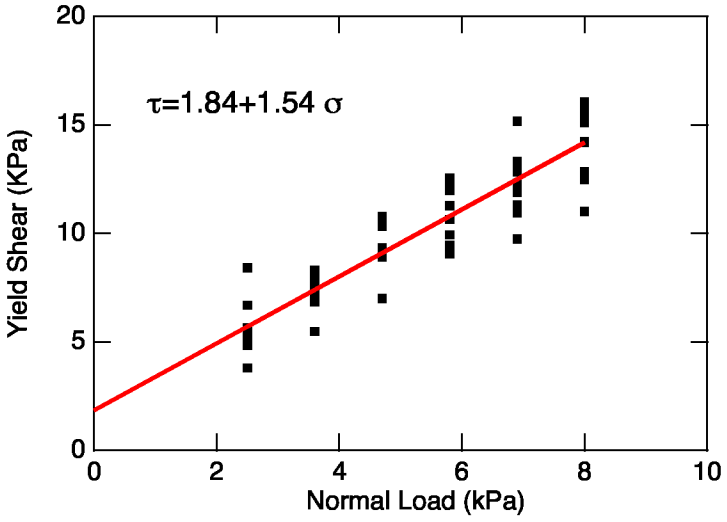

Figure 8: Static yield locus with 3-min consolidation in vibration table at $\sigma_c = 10$ kPa. Cohesion ≈ 1.84 kPa and $\phi \approx 57°$.

"dynamic" friction force. Fig. 9 shows the time plot of a typical dynamic yield locus. When the analysis begins, at $t \approx 110$ sec, the vertical head rises at constant speed. The normal force decreases monotonically (this is not always the case; it rises in some experiments, see below) but not linearly. The shear force does not decrease monotonically; it rises a bit several times (see, e.g., $t \approx 127$ sec and at $t \approx 135$ sec).

Fig. 10 shows 10 typical dynamic yield loci, for 10 kPa pre-consolidation pressure. The spread in the data is larger than in the conventional static yield locus. In order to understand this and the anomalies noted in the previous paragraph, we need to examine how the dynamic yield locus is measured. Once the sample is in steady state, the normal force begins to drop across the range required for the particular yield locus. In the ShearScan instrument, the normal force is not controlled directly; instead, the vertical head position is raised at a fixed rate. This, ideally, would cause the normal force to drop monotonically in time, assuming the sample expands in sync with the vertical head motion. This is not always the case in the dynamic test. In some runs, the normal and shear stresses increase together for short periods of time even during the head's upward motion. This is likely the result of sample dilation events happening at expansion rates larger than the rate of upward motion of the vertical head. The granular material jams momentarily while some particles have to roll over others as the rotation is forced to proceed.

3.4 Wall yield locus

This test is analogous to the Static Yield Locus, except that the yield points are measured as though they were a succession of "steady states" without re-conditioning between failure points. Fig. 11 shows a typical time plot taken at 10 kPa consolidation. The first friction value is taken at 10 kPa normal load. For each successive

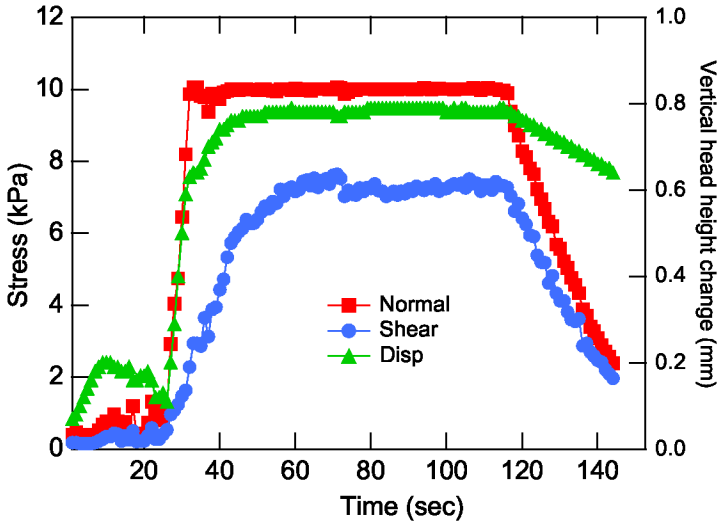

Figure 9: Normal and shear stresses, and sample height change, versus time during a Dynamic yield locus. $\sigma_c = 10$ kPa. Yield locus data is taken at $t > 117$ sec. Vertical head rise rate (▲) is constant but normal stress (■) and shear stress (●) rates of change are not.

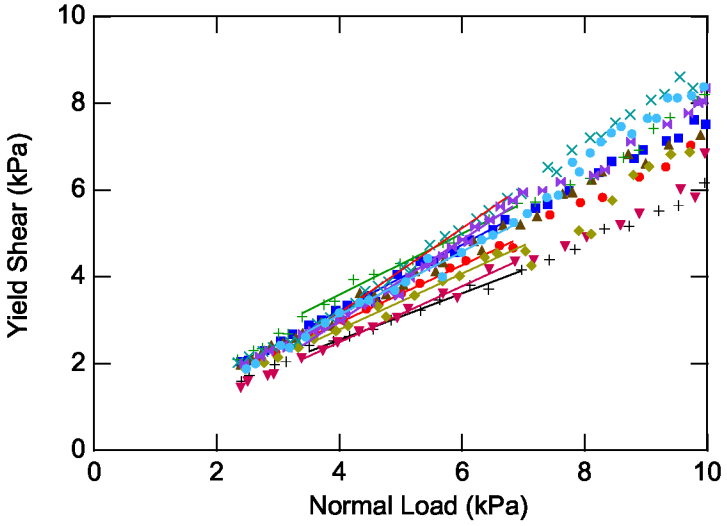

Figure 10: Dynamic YL for $\sigma_c = 10$ kPa. Ten individual YL are shown with their respective best straight fits to illustrate run-to-run variability.

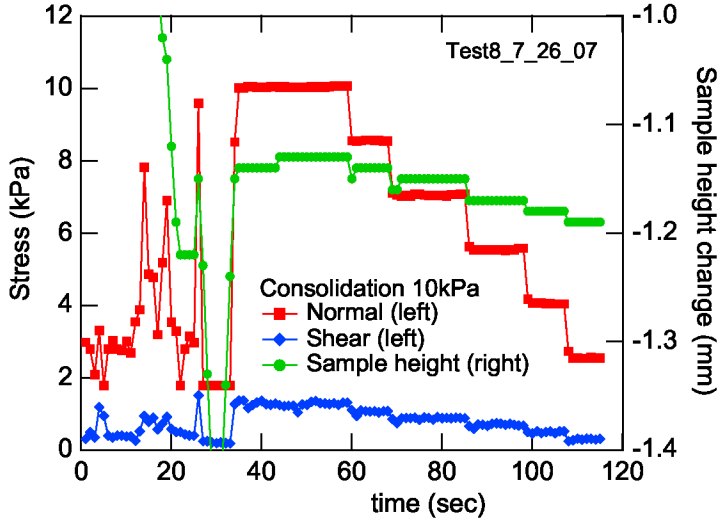

Figure 11: Time plot of stainless steel wall friction at $\sigma_c = 10$ kPa.

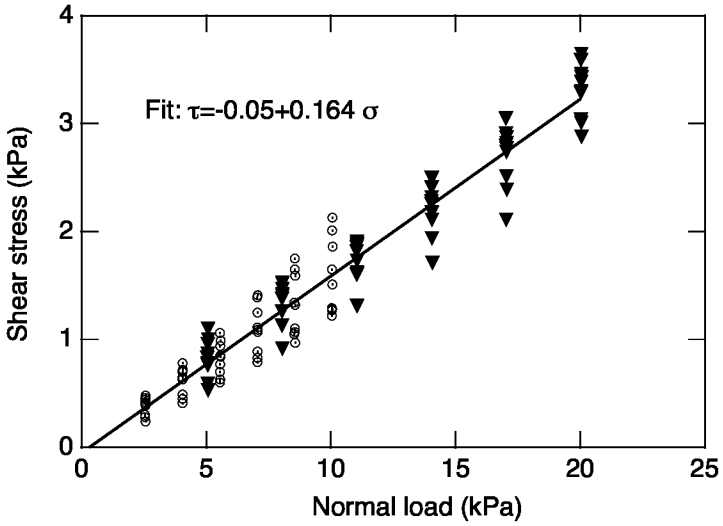

Figure 12: Wall yield locus of stainless steel at $\sigma_c = 20$ kPa (solid triangles) and 10 kPa (clear circles).

friction point, the normal load is dropped and the corresponding shear stress (friction) measured. Fig. 11 also shows that the sample dilates as the normal load decreases. Since the powder is not deformed in this test, τ does not grow in time as in the yield points of a deforming material (cf. fig. 7). Fig. 12 shows the yield locus corresponding to fig. 11. Friction data for $\sigma_c = 20$ kPa are plotted in the same figure and follow the same trend as the data for $\sigma_c = 10$ kPa.

4 Discussion

4.1 Data analysis

In tables 1-5 we summarize the different types of test we performed, highlighting the number of repetitions for each data point, and the standard deviation associated with each value. One goal was to quantify the test-to-test variability and, in particular, to be able to assess when a material is effectively cohesionless –i.e., when it has zero cohesion. Clearly, the answer depends on the average and standard deviation of a material's cohesion across many independent measurements and, consequently, each new material must be characterized in this manner to quantify uncertainties and understand the method's precision.

4.2 Static yield loci

Tables 1 and 3 show that cohesion is an increasing function of consolidation load. However, the internal angle of friction and the bulk density do not exhibit a clear correlation with consolidation load.

Table 1: Static yield locus (no time-consolidation). N is number of repetitions, ρ is bulk density and R is the ratio of standard deviations of MCS and UYS.

σ_c	N	UYS (kPa)	MCS (kPa)	ϕ (deg)	c (kPa)	ρ (g/cm^3)	R
2.5	10	0.11 ± 0.38	4.53 ± 0.26	40.49 ± 3.77	0.03 ± 0.09	1.68±0.03	0.68
5	9	0.59 ± 0.38	9.20 ± 0.40	39.91 ± 2.47	0.14 ± 0.10	1.68±0.03	1.05
10	9	1.52 ± 0.58	18.88 ± 0.80	39.59 ± 1.65	0.36 ± 0.13	1.68±0.03	1.38
20	10	1.57 ± 2.55	39.49 ± 2.12	40.04 ± 2.18	0.38 ± 0.60	1.69±0.03	0.83

Table 2: Dynamic yield locus

σ_c	N	UYS (kPa)	MCS (kPa)	ϕ (deg)	c (kPa)	ρ (g/cm^3)
2.5	10	0.05 ± 0.47	5.62 ± 0.75	36.44 ± 5.01	0.02 ± 0.12	1.51 ± 0.11
5	10	0.77 ± 0.53	11.54 ± 0.98	33.18 ± 2.99	0.21 ± 0.15	1.57 ± 0.1
10	10	0.13 ± 2.03	24.27 ± 3.30	35.93 ± 4.78	0.07 ± 0.47	1.58 ± 0.1
20	10	2.59 ± 2.82	45.10 ± 4.21	32.67 ± 3.05	0.71 ± 0.76	1.59 ± 0.1

4.3 Typical flow functions for vibration-consolidated and conventionally failed samples

Flow function is a plot of unconfined yield strength versus major consolidation stress. The flow function is an indicator of how easily a material flows. In general, the higher

Table 3: Static yield locus with vibration time-consolidation

σ_c	N	UYS (kPa)	MCS (kPa)	ϕ (deg)	c (kPa)	ρ (g/cm^3)
2.5	10	5.12 ± 3.86	25.44 ± 15.38	65.75 ± 4.49	0.62 ± 0.90	1.97 ± 0.07
5	10	11.03 ± 0.80	50.96 ± 8.02	65.89 ± 1.32	1.33 ± 0.40	1.97 ± 0.06
10	10	12.42 ± 0.63	68.31 ± 7.27	60.03 ± 1.06	1.84 ± 0.48	1.92 ± 0.07
20	10	45.74 ± 2.34	241.7 ± 39.9	67.71 ± 1.28	5.00 ± 1.89	2.0 ± 0.04

Table 4: Aluminum Wall yield locus

σ_c (kPa)	Repetitions	ϕ (deg)	c (kPa)
2.5	10	23.03 ± 1.36	-0.12 ± 0.03
5	10	24.95 ± 2.37	-0.10 ± 0.12
10	10	22.23 ± 1.70	0.05 ± 0.23
20	10	20.67 ± 1.43	0.19 ± 0.31

Table 5: Stainless Steel Wall yield locus

σ_c (kPa)	Repetitions	ϕ (deg)	c (kPa)	Coupon
2.5	10	15.81 ± 3.54	-0.01 ± 0.09	new
5	10	13.88 ± 1.68	0.09 ± 0.07	new
5	10	8.69 ± 1.39	-0.06 ± 0.05	old
10	10	8.74 ± 2.63	-0.01 ± 0.17	old
20	10	9.22 ± 1.03	-0.01 ± 0.28	old

the flow function (i.e., the higher the strength) the less flowable the material, all else being kept constant. There may be cases when the flow functions for two materials intersect at a particular value of major consolidation stress, MCS^*. In that case, one material flows better when $MCS < MCS^*$, and the other material flows better when $MCS > MCS^*$.

Fig. 13 shows the flow function of the Static yield locus. The figure shows individual values for each of the 10 repetitions done for each yield point. The variability in the 20 kPa values is larger than the others but it is not excessive when measured as a ratio R of the MCS to UYS standard deviations. This flow function is typical of an easy-flowing, low-cohesion material. Fig. 14 shows the flow functions of the static, dynamic and vibration-consolidated yield loci. The first observation is that the dynamic and static flow functions are indistinguishable from one another. The second, and more important, observation is that the vibration-consolidated flow function corresponds to a much less flowable material than the conventionally prepared material samples. We will see how this flow property impacts the hopper design below.

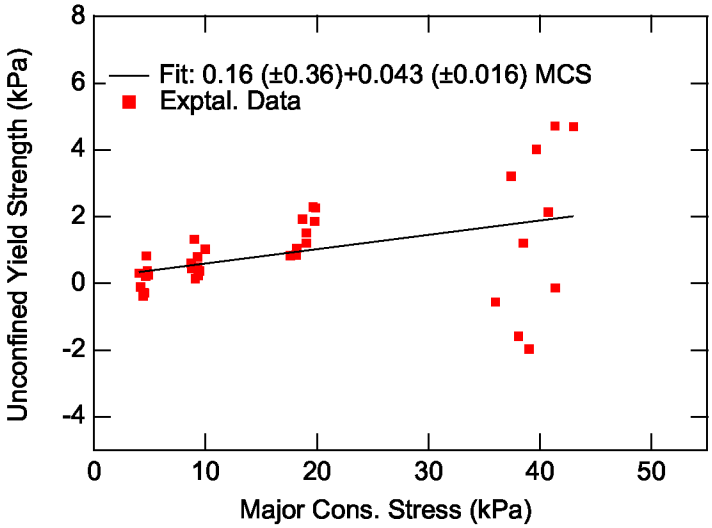

Figure 13: Flow function for the Static YL showing all the data repetitions at each consolidation pressure. From left to right, the point clusters correspond to $\sigma_c = 2.5$ kPa, 5 kPa, 10 kPa and 20 kPa.

The observed differences in flow function between vibration-consolidated material and material failed without time consolidation are a consequence of the differences in strength (or yield loci) between the two types of material. Examination of figs. 4 and 8 shows that the cohesion and angle of friction are both higher in the vibration-consolidated samples. This trend, illustrated here for $\sigma_c = 10$ kPa, is also observed in yield loci at the other consolidation values $\sigma_c = 2.5, 5$ and 20 kPa.

4.4 Effect of the environment

The tests reported here were carried out without any special effort to control the atmospheric moisture. The tests spanned a few months, starting in the winter of 2006-2007 and ending in the summer of 2007. It is likely that the relative humidity varied significantly between winter and summer when the tests were completed. However, test repetitions performed in different seasons fall within the test-to-test variability, determined by repeating the test 9 or 10 times in the span of one or two days, where seasonal variations are not an issue. Thus, we expect that moisture effects on powder shear strength are likely smaller than test-to-test variations caused by such factors as sampling and sample preparation.

4.5 Hopper design for mass flow

All measurements presented in section 3 show a complete characterization of the JSC-1a simulant with an outlook to determining its flowability and, then, a hopper design for "mass flow", where this term denotes a flow condition devoid of stagnant powder regions. The design method ensures that, at the hopper outlet, the stress exerted on

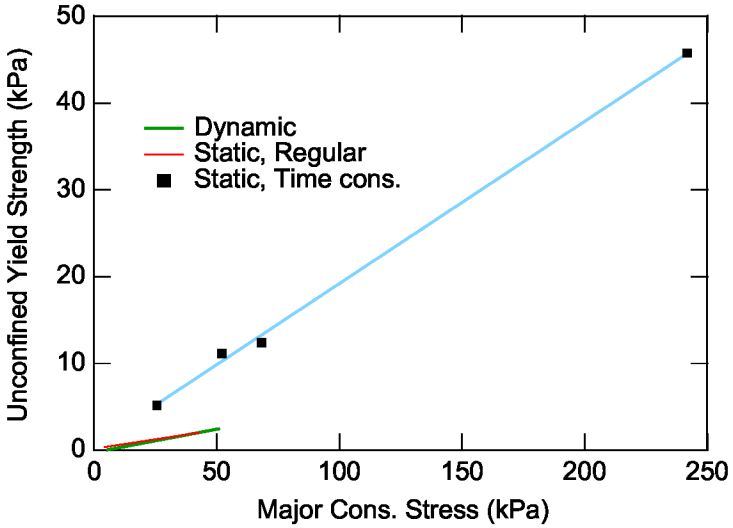

Figure 14: Flow functions for Static YL (red) dynamic YL (green) and time-YL with vibration consolidation (black symbols). The latter is significantly less flowable than either of the other two –among which there is no significant difference.

the material (from the material standing above it) exceeds its strength (determined by the consolidation state caused by forces exerted by the material above).

A crucial parameter in the design is the ratio of the major consolidation stress, MCS, to the minimum stress at an arch formed in the hopper outlet, denoted as S. In conical or wedge (planar) hopper geometries, this ratio only depends on cone (or wedge) angle and is called "flow factor", $ff \equiv MCS/S$.

As the flow function of fig. 14 shows, as the material is compressed with normal stress MCS, it develops strength. At the hopper outlet, this strength is "unconfined", denoted here as UYS, because one of the two principal stresses is zero there. The key in the design is to find conditions where the minimum stress at the outlet is larger than the strength, $S > UYS$. A line plotted in the flow function graph passing through zero and with slope $1/ff$ represents the state of stress of the powder at the hopper outlet as a function of consolidation stress MCS. Its intersection with the flow function determines a critical consolidation stress MCS^*. To ensure $S > UYS$ (i.e., stress $>$ strength)we must then have $MCS > MCS^*$. The design cycle will determine the orifice size and cone angle to ensure this condition is met.

We begin by outlining the sequence of steps in a typical design cycle. First, the "effective friction angle", δ, of the powder is determined at each consolidation σ_c as the slope of the straight line in the yield locus passing through zero and tangent to the Mohr circle that determines the major consolidation stress, MCS. A plot of δ vs. MCS is then made.

As is common in engineering practice, the design is iterative. The rule of thumb is to assume $ff_1 = 1.3$ to start the first iteration (the subscript 1 refers to the iteration number). A value of MCS_1^* is found from the intersection of the flow function line with the line $S = MCS/ff$. Knowing MCS_1^* we may find $\delta_1^* = \delta(MCS_1^*)$ from the

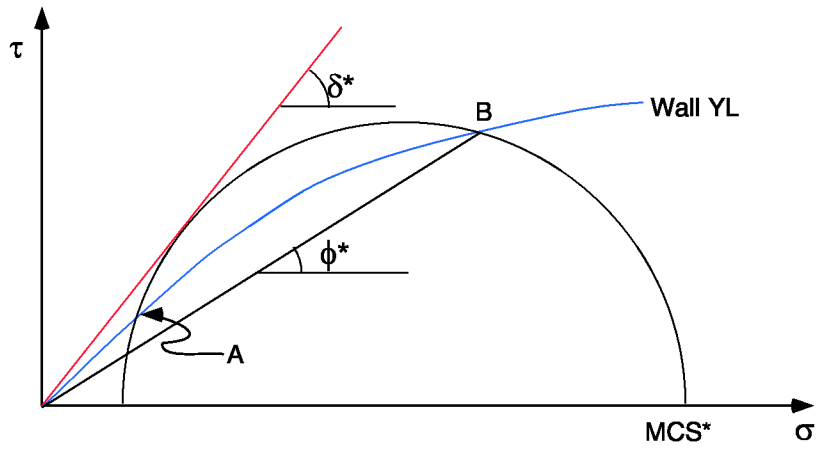

Figure 15: Construction to determine the kinematic angle of wall friction, ϕ'.

plot of δ vs. MCS made already.

On the wall yield locus, we draw a line with angle δ_1^* to the horizontal, and then the Mohr circle with major principal stress MCS_1^* and tangent to the δ_1^*-line, refer to fig. 15. A safe value of the kinematic angle of wall friction, $\phi_1'^*$, is given by the slope of the line between zero and point B in the construction of the same figure [1].

Mathematical analysis of the stress field in cone (and wedge) geometries yields plots of ϕ' vs. cone angle θ_c; the lines are parametrized by the flow factor ff, and shown schematically in fig. 16 [1]. Using $\phi' = \phi_1'^*$, we find the maximum cone angle where mass flow solutions exist, θ_c^*. A safety factor of 4° is subtracted, so the cone angle is chosen to be $\theta_c^* - 4°$. The point in the figure $[\phi_1'^*, (\theta_c^* - 4°)]$ lies on a line with flow factor ff_1'. Typically, $ff_1' \neq ff_1$, so the initial assumed value of the flow factor is updated to $ff_2 = ff_1'$ and the design cycle goes into iteration 2. Usually, two iterations are sufficient for engineering purposes.

Once the cone angle, θ, has been found, the orifice size is obtained as follows. With ff known from a converged iteration process, the converged critical stress MCS^* and strength S^* may be found from the intersection of the flow function with the straight line passing through zero with slope $1/ff$. Then, the opening span B (diameter for conical and width for wedge hoppers) is found from

$$B = \frac{SH(\theta)}{\rho_b g}, \tag{2}$$

where ρ_b is bulk density and g is the acceleration of gravity. $H(\theta)$ is a function found plotted in fig. 43 of ref. [1] for both circular and wedge hoppers. For small angles, $H_{\text{circ}} \approx 2$ and $H_{\text{wedge}} \approx 1$.

Table 6 shows design parameters for two different wall materials (aluminum and stainless steel) and two consolidation procedures (pre-shear and shaker table). The orifice diameter, which is mainly controlled by cohesion, is rather uniform across materials because cohesions are modest in both the vibration and pre-shear consolidated powders. Furthermore, the freely-poured JSC-1a is cohesionless and, therefore, $MCS^* = 0$. In such a case, the orifice size must be fixed from considerations of

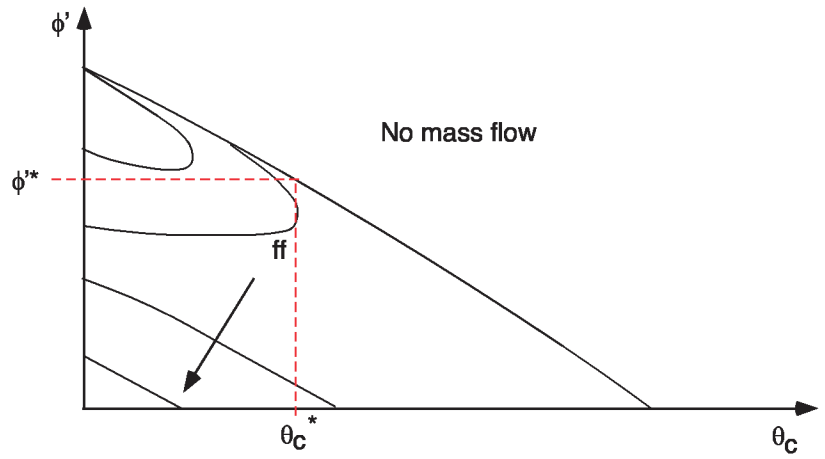

Figure 16: Construction to determine cone angle, θ_c. Schematic based on graphs appearing in reference [1]. The parameter in the lines is the flow factor, ff, which increases downward as indicated by the arrow.

flow rate and arching [28], to then determine the cone angle in the usual way [1]. We decided to try a design using the same orifice diameter that we found for the vibration-consolidated powder, a safe assumption for a cohesionless powder. The cone angles, on the other hand, are mainly controlled by wall-powder friction –a result of wall finish/roughness and wall hardness– and differ significantly with wall material. In our case, the aluminum wall has an average finish ($R_a \approx 25$ μin) and the stainless steel has a "mirror" finish ($R_a \approx 3-5$ μin). As a result, the aluminum requires a steeper cone than the stainless steel.

Table 6: Design parameters for mass flow of JSC-1a in a conical hopper

Wall Material	Finish	Powder Consolidation	Cone angle 2θ, (°)	Orifice Diameter (cm)
Aluminum	Average	Vibration	38	13
Stainless Steel	Mirror	Vibration	66	14
Aluminum	Average	Pre-shear	37	15
Stainless Steel	Mirror	Pre-shear	76	17

5 Summary

We have characterized JSC-1a's flowability following the methods developed by Jenike [1]. Using Sci-Tec's ShearScan instrument, we have followed closely the standard developed in ASTM-6773. We have developed an alternative, non-standard test with time consolidation on a vibration table and without pre-shear. The suite of tests we carried out is necessary for the construction of flow functions and, thus, allow one to

design a hopper for flow of the tested material. Past work where soil strength has been measured with triaxial and rotational methods does not comprise a useful suite of measurements necessary for hopper design, for example, it does not subject the soil to steady-state pre-shear before each yield point.

The material failed when pre-sheared with undetectable cohesion and an internal friction angle close to 40 ± 4 degrees. By contrast, the vibrated sample taken to failure without preshear showed a small but non-zero cohesion which increased with consolidation pressure, and a significantly higher internal friction angle in the range from 60 to ≈ 68 degrees.

The flowability, as measured by the flow functions with pre-shear and without, shows marked differences, with the vibrated no-preshear material being a lot less flowable. This decreased flowability is associated with the higher cohesion and internal friction angle which yield a flow function everywhere above the one for the pre-sheared powder.

Finally, we recall that reproducing lunar gravity conditions in a terrestrial laboratory may not be possible if the soil strength depends on gradients (or higher derivatives) of the normal load. Furthermore, our own flowability measurements show marked differences dependent on the material preparation –or history. It is impossible to know the precise compaction history of lunar regolith to be encountered on the Moon. Thus, designs –not only of hoppers but of soil-moving equipment as well– should take a conservative approach when considering the likely regolith's strength and consolidation state.

From an engineering point of view, it is important to keep in mind the following points:

1. Powder-wall friction controls hopper angle; cohesion controls aperture size.

2. Yield loci are curved, particularly near $\sigma = 0$. Thus, resolution near $\sigma = 0$ is necessary; and extrapolation to $\sigma = 0$ from higher values of σ is questionable.

3. Pre-shear is the industrial standard for bulk powder flow and has not been done in the soil mechanics of lunar simulant/regolith.

4. c, ϕ are not material properties, but their values and cross-correlations depend on actual material properties at the particle level.

5. Hopper design is an iterative, manual and graphical process that is grounded on the analysis of stress in the powder residing in the hopper.

6. Dynamic yield locus is related to the stress below which flow stops; static yield locus is related to the stress above which flow takes place.

7. Onset of flow of a consolidated powder necessitates powder dilation.

6 Appendix

We now present formulas to compute the major consolidation stress and unconfined yield strength. From the construction in fig. 1, it is possible to show that

$$MCS = -\frac{c}{\tan\phi} + (1+\sin\phi)\frac{A - \sqrt{A^2\sin^2\phi - \tau_s^2\cos^2\phi}}{\cos^2\phi} \tag{3}$$

$$UCY = 2\,c\,\frac{1+\sin\phi}{\cos\phi}, \tag{4}$$

where $A \equiv \sigma_s + c/\tan\phi$, and (σ_s, τ_s) are respectively the normal and shear stress values at the steady state pre-shear point.

For completeness, we present the minor stress intersection of the Mohr circle giving the MCS, denoted as σ_2:

$$\sigma_2 = -\frac{c}{\tan\phi} + (1-\sin\phi)\frac{A - \sqrt{A^2\sin^2\phi - \tau_s^2\cos^2\phi}}{\cos^2\phi}. \tag{5}$$

References

[1] A.W. Jenike. Storage and flow of solids. Bulletin No. 123 of the Utah Experimental Station, University of Utah, Salt Lake City, Utah, November 1964.

[2] E.W. Merrow. A Quantitative Assessment of R&D Requirements for Solids Processing Technology. Report R-3216-DOE/PSSP, Rand Corporation, 1986.

[3] R.A Wilkinson, R.P. Behringer, J.T Jenkins, and M.Y. Louge. Granular materials and the risks they pose for success on the moon and mars. In *at Space Technology & Application International Forum 2005 (STAIF05)*, Albuquerque, NM, February 2005.

[4] Mieczyslaw Gregory Bekker. *Theory of Land Locomotion.* University of Michigan Press, Ann Arbor, 1956.

[5] J.K. Mitchell, W.N. Houston, W.D. Carrier, III, and N.C. Costes. Apollo soil mechanics experiment s-200. Space Sciences Laboratory Series Series 15, Issue 7, Univ. of California at Berkeley, 1974.

[6] W.D. Carrier, III, L.G. Bromwell, and R.T. Martin. Strength and compressibility of returned lunar soil (Apollo 12 soil sample strength, compressibility, bulk density, porosity, and shear wave velocity). In *Lunar Science Conference, 3rd*, pages 3223–3234, January 1972.

[7] L.G. Bromwell, W.D. Carrier, III, N.C. Costes, J.K. Mitchell, and R.F. Scott. Soil mechanics experiment (Lunar soil mechanics and properties based on Apollo 14 observations and data). Preliminary science report, MIT, 1971.

[8] W.D. Carrier, III, L.G. Bromwell, and R.T. Martin. Behavior of returned lunar soil in vacuum. *ASCE Journal of the Soil Mechanics and Foundations Division*, 99(SM11, Proc. Paper 10156):979–996, November 1973.

[9] W.D. Carrier, III. Lunar soil grain size distribution. *The Moon*, 6(3-4):250–263, April 1973.

[10] W.D. Carrier, III, J.K. Mitchell, and A. Mahmood. The nature of lunar soil. *ASCE, Journal of the Soil Mechanics and Foundations Division*, 99:813–832, October 1973.

[11] N.C. Costes, W.D. Carrier, III, J.K. Mitchell, and R.F. Scott. Apollo 11: Soil mechanics results. *Journal of the Soil Mechanics and Foundations Division.*, 96(6):2045–2080, November 1970.

[12] R.F. Scott, W.D. Carrier, III, N.C. Costes, and J.K. Mitchell. Apollo 12 soil mechanics investigation. *Geotechnique*, 21(1):1–14, 1971.

[13] John David Nelson. *Environmental effects on engineering properties of simulated lunar soils.* PhD thesis, Illinois Institute of Technology, Chicago, Illinois, 1967.

[14] D.E. Nicholson. *Gravity flow of powder in a lunar environment. 1: Property determination of simulated lunar soil (Analysis of mechanical behavior of fine soils in lunar environment and application to engineering design of gravity-flow bins).* Number RI 7543. U.S. Bureau of Mines, 1971.

[15] William G. Pariseau and David E. Nicholson. Gravity flow bin design for lunar soil. In *Proceedings of the 2nd Symposium on Storage and Flow of Solids*, pages 1–8, Chicago, IL, 1972. ASME.

[16] Susan N. Batiste and Stein Sture. Lunar Regolith Simulant MLS-1: Production and Engineering Properties. In *Book of Abstracts: Lunar Regolith Simulant Materials Workshop*, pages 101–103. NASA, Marshall Space Flight Center, February 1-2, 2005.

[17] X. Zeng, C. He, H. Oravec, A. Wilkinson, J. Aguí, and V. Asnani. Geotechnical Properties of JSC-1A Lunar Soil Simulant. *ASCE J. Aerosp. Eng.*, submitted.

[18] Haydar Arslan and Susan Batiste. JSC-1a Geotechnical Properties Experiments; Tons 1, 2, 3. Technical Report 105525, Laboratory For Atmospheric and Space Physics, University of Colorado, 2007.

[19] W.A. Beverloo, H.A. Leniger, and J. Van de Velde. The flow of granular material through orifices. *J. Chem. Eng. Sci.*, 15:260–296, 1961.

[20] C. Mankoc, A. Janda, R. Arévalo, J.M. Pastor, I. Zuriguel, A. Garcimartín, and D. Maza. The flow rate of granular materials through an orifice. *Granular Matter*, 9:407–414, 2007.

[21] *Proceedings of the Fifth world congress on particle technology.* AIChE, Orlando, FL, April 2006; ISBN: 0-8169-1005-7 P-227.

[22] C.-A. Coulomb. Essai sur une application des règles de maximis et minimis à quelques problèmes de statique, relatifs à l'architecture. In *Mémoires de mathématiques et de physique, présentés à l'Académie Royale des Sciences, par divers sçavans, et lus dans ses assemblées en 1773*, volume 7, pages 343–382, Paris, 1776. Impr. Royale.

[23] S.P. Timoshenko and J.N. Goodier. *Theory of Elasticity*, pages 19–22. McGraw-Hill, 1970. (see also O. Mohr, Zivilingenieur, 1882, p. 113).

[24] B.M. Willman, Boles W.W., McKay D.S., and Allen C.C. Properties of lunar soil simulant JSC-1. *J. Aerospace Eng.*, 8(2):77–87, 1995.

[25] J.J. Fitzpatrick, S.A. Barringer, and T. Iqbal. Flow property measurement of food powders and sensitivity of Jenike's hopper design methodology to the measured values. *Journal of Food Engineering*, 61:399–405, 2004.

[26] A. Castellanos, J.M. Valverde, and M.A.S. Quintanilla. The sevilla powder tester: A tool for characterizing the physical properties of fine cohesive powders at very small consolidations. *KONA*, 22:66–81, 2004.

[27] Orbital Technologies Corporation. Material safety data sheet, 2005. 1212 Fourier Dr., Madison WI 53717, http://www.lunarmarssimulant.com.

[28] John Carson. Personal communication, 2007. Jenike & Johanson.

REPORT DOCUMENTATION PAGE	Form Approved OMB No. 0704-0188

1. REPORT DATE *(DD-MM-YYYY)*	2. REPORT TYPE	3. DATES COVERED *(From - To)*
01-05-2009	Technical Memorandum	

4. TITLE AND SUBTITLE
Flowability of JSC-1a

5a. CONTRACT NUMBER

5b. GRANT NUMBER

5c. PROGRAM ELEMENT NUMBER

6. AUTHOR(S)
Rame, Enrique; Wilkinson, Allen; Elliot, Alan; Young, Carolyn

5d. PROJECT NUMBER

5e. TASK NUMBER

5f. WORK UNIT NUMBER
WBS 387498.04.01.01.02.03

7. PERFORMING ORGANIZATION NAME(S) AND ADDRESS(ES)
National Aeronautics and Space Administration
John H. Glenn Research Center at Lewis Field
Cleveland, Ohio 44135-3191

8. PERFORMING ORGANIZATION REPORT NUMBER
E-16938

9. SPONSORING/MONITORING AGENCY NAME(S) AND ADDRESS(ES)
National Aeronautics and Space Administration
Washington, DC 20546-0001

10. SPONSORING/MONITORS ACRONYM(S)
NASA

11. SPONSORING/MONITORING REPORT NUMBER
NASA/TM-2009-215625

12. DISTRIBUTION/AVAILABILITY STATEMENT
Unclassified-Unlimited
Subject Category: 23
Available electronically at http://gltrs.grc.nasa.gov
This publication is available from the NASA Center for AeroSpace Information, 301-621-0390

13. SUPPLEMENTARY NOTES

14. ABSTRACT
We have done a complete flowability characterization of the lunar soil simulant, JSC-1a, following closely the ASTM-6773 standard for the Schulze ring shear test. The measurements, which involve pre-shearing the material before each yield point, show JSC-1a to be cohesionless, with an angle of internal friction near 40°. We also measured yield loci after consolidating the material in a vibration table which show it to have significant cohesion (≈1 kPa) and an angle of internal friction of about 60°. Hopper designs based on each type of flowability test differ significantly. These differences highlight the need to discern the condition of the lunar soil in the specific process where flowability is an issue. We close with a list--not necessarily comprehensive--of engineering rules of thumb that apply to powder flow in hoppers.

15. SUBJECT TERMS
Granular materials

16. SECURITY CLASSIFICATION OF:			17. LIMITATION OF ABSTRACT	18. NUMBER OF PAGES	19a. NAME OF RESPONSIBLE PERSON
a. REPORT	b. ABSTRACT	c. THIS PAGE			STI Help Desk (email:help@sti.nasa.gov)
U	U	U	UU	32	19b. TELEPHONE NUMBER *(include area code)* 301-621-0390